BUILDING RESEARCH JOURNAL
VOLUME 60, 2012 NUMBER 3 – 4

MESHLESS MLPG APPROACH FOR THE ANALYSIS OF PIEZOELECTRIC SENSORS UNDER COMPRESSIVE LOAD

PETER STANAK[1], ANTONIO TADEU[2], JAN SLADEK[1] AND VLADIMIR SLADEK[1]

The paper presents a numerical analysis of a three-dimensional piezoelectric solid using the meshless local Petrov-Galerkin (MLPG) method. The mechanical and electrical response of a piezoelectric sensor is investigated for a static and transient compressive load. In the proposed meshless formulation nodal points are uniformly distributed in the analyzed domain, but without loss of generality. Each node is the center of a small spherical subdomain. The local integral equation (LIE) formulation is derived from the equations of motion for the mechanical fields and quasi-static Maxwell's equations on the appropriate subdomains. The unit step function is used as a test function in derivation of the LIEs. The moving least-squares (MLS) method is used to approximate the spatial variations of all physical fields. The Houbolt finite difference scheme is used to solve a time-dependent system of ordinary differential equations for mechanical displacements and electric potential.

Keywords: piezoelectric sensor, meshless local Petrov-Galerkin method, moving least-squares approximation, Houbolt method

1. Introduction

Piezoelectric materials have found a wide range of applications over the last two decades, in the fields of aerospace, naval, automotive, civil engineering and medicine. This is because their sensory/active capabilities enable them to convert mechanical energy into electric energy and vice-versa. A piezoelectric element will generate electrical disturbance if a mechanical load is applied to its surface in the poling direction. Thus, by varying the mechanical input the electrical response (output) is changed and can be easily detected. Structures incorporating smart piezoelectric materials are often referred to as adaptive or intelligent structures. Distributed piezoelectric sensors and actuators are important for the active vibration control or structural monitoring of various elastic structures. A typical piezoelectric sensor is shown in Figure 1. Piezoelectric actuators are the key element for controlling and suppressing structural deformations (Adachi et al., 1994). Application of piezoelectric sensors to structural health monitoring (SHM) or displacement and vibration sensing is attracting increased attention (Song, Sethi and Li, 2006). New engineering applications are emerging that offer significant research interest in the field of computer modeling and applied mechanics.

[1] Institute of Construction and Architecture, Slovak Academy of Sciences, 845 03 Bratislava, Slovak Republic, e-mail: perter.stanak@savba.sk, jan.sladek@savba.sk, vladimir.sladek@savba.sk
[2] ITeCons, University of Coimbra, Pólo II, Rua Pedro Hispano, 3030-289, Coimbra, Portugal

Analytical solutions for piezoelectric structures are available only for simple boundary conditions (Heyliger, 1997). Ray, Bhattacharya and Samanta (1998) developed an analytical solution for laminated composite plates with active piezoelectric layers, but at the cost of high mathematical complexity. Vel and Batra (2000) devised an analytical solution for multilayered piezoelectric plates in terms of the double Fourier series to handle more general boundary conditions at the edges.

Figure 1. Typical circular piezoelectric sensor

Advanced numerical methods are needed to solve boundary value problems involving piezoelectric phenomena, due to their mathematical complexity. The finite element method (FEM) is a dominant numerical technique for solving complex engineering problems. The FEM has been increasingly used to solve piezoelectric problems (Allik & Hughes, 1970; Benjeddou, 2000; Semedo Garcao et al., 2004). The boundary element method (BEM) is an efficient and popular alternative to the FEM. The BEM only requires construction of the mesh on the boundary of the analyzed domain, thus significantly reducing time-consuming mesh generation. However, it requires a fundamental solution or Green's functions that are unavailable for 3-D problems in piezoelectric anisotropic materials. Therefore, the application of the BEM is restricted to a relatively small group of engineering problems where a fundamental solution is available. Several applications of BEM to problems involving piezoelectricity have been reported (Lee, 1995; Ding and Liang, 1999). The BEM has been successfully used for general crack analysis in piezoelectric solids, too [Pan, 1999; Davi and Milazzo, 2001; Garcia-Sanchez et al., 2007].

The meshless modeling of a broad range of engineering problems has recently become very attractive for many researchers (Atluri and Sladek, 2009; Nguyen et al., 2008) as an alternative to the well-established mesh-based methods (FEM, BEM). Meshless methods do not require discretization using the finite element mesh, which offers certain advantages. For example problems including shear locking of elements or expensive mesh generation in the finite element method (FEM) or unavailable fundamental solution in the boundary element method (BEM) are effectively eliminated in meshless methods. The meshless Local Petrov-Galerkin (MLPG) method (Atluri, 2004) is one of the most popular meshless methods as it does not require the creation of a mesh for the approximation or integration of unknown quantities. Thus it can be said to be a "truly meshless" method.

The MLPG method has been successfully applied to the analysis of a broad range of engineering problems including the elastic analysis of general 3-D solids (Sladek et al. 2009), bending of thin and thick plates (Sladek et al., 2003; Soric and Jarak, 2010) or fracture problems (Ching and Batra, 2001). Papers related to solving piezoelectric problems using the MLPG involve analyzing axisymmetric continuously non-homogeneous piezoelectric solids (Sladek et al. 2008), rectangular piezoelectric plates (Sladek et al. 2010), functionally graded circular plates (Sladek et al. 2013) and composite circular plates under transient loading (Stanak et al. 2011).

This paper describes the application of the MLPG method to the 3-D analysis of a piezoelectric sensor under a compressive load. The cylindrical sensor is discretized with nodal points only, and

a small spherical subdomain is introduced around each nodal point. The coupled electro-mechanical fields in piezoelectric material are described by constitutive relations and governing partial differential equations (PDE). Local integral equations constructed from the weak form of governing PDEs are defined over these local subdomains. A moving least-squares (MLS) approximation scheme (Lancaster and Salkauskas, 1981) is used to approximate the spatial variations of unknown field variables and the Heaviside unit step function is used as a test function. The essential boundary conditions are satisfied by the collocation of MLS approximation expressions for unknowns on the boundary nodes. After performing the spatial MLS approximation, a system of ordinary differential equations for certain nodal unknowns is obtained. Then, the system of the ordinary differential equations of the second order resulting from the equations of motion is solved by the Houbolt finite-difference scheme (Houbolt, 1950) as a time-stepping method. Numerical examples are presented for different loading scenarios that can appear when the sensor is loaded with a non-uniform loading pattern. Final conclusions and a comparison with FEM data obtained by the ANSYS commercial code are discussed.

2. Local integral equations and the MLPG formulation

The behavior of a general piezoelectric body is mathematically described by a set of governing equations and constitutive equations. The governing equations for general 3-D piezoelectric solid under quasi-electrostatic assumption are given by the equation of motion for elastic displacements u_i and the first Maxwell's equation of electrostatics for the vector of electric displacements D_i as

$$\sigma_{ij,j}(\mathbf{x},t)+X_i(\mathbf{x},t)=\rho(\mathbf{x})\ddot{u}_i(\mathbf{x},t) \tag{1}$$

$$D_{i,i}(\mathbf{x},t)-R(\mathbf{x},t)=0 \tag{2}$$

where t, σ_{ij}, X_i, R, ρ are the time, stresses, vector of body forces, volume density of free electric charges and mass density, respectively. The dots over a quantity indicate the time derivative. Neglecting the acceleration term in Eq. (1) one can easily transform the dynamic problem into a static one. The piezoelectric constitutive equations given by Tiersten (1969) are expressed as converse and direct linear piezoelectric equations, respectively

$$\sigma_{ij}(\mathbf{x})=C_{ijkl}\varepsilon_{kl}(\mathbf{x})-e_{kij}E_k(\mathbf{x}) \tag{3}$$

$$D_i(\mathbf{x})=e_{ikl}\varepsilon_{kl}(\mathbf{x})+h_{ik}E_k(\mathbf{x}) \tag{4}$$

where C_{ijkl}, e_{kij}, h_{ik} represent the elastic, piezoelectric and dielectric material coefficients, respectively. Cartesian coordinates are specified as $\mathbf{x} = (x_1,x_2,x_3)$. The strain tensor ε_{ij} and electric field vector E_k are related to mechanical displacements u_i and electric potential ψ by

$$\varepsilon_{ij}=\frac{1}{2}\left(u_{i,j}+u_{j,i}\right) \tag{5}$$

$$E_k=-\psi_{,k} \tag{6}$$

The following essential and natural boundary conditions are assumed for the mechanical field

$$u_i(\mathbf{x},t) = \tilde{u}_i(\mathbf{x},t) \text{ on } \Gamma_u$$
$$\sigma_{ij} n_j = \tilde{T}_i(\mathbf{x},t) \text{ on } \Gamma_t \tag{7}$$

and for the electrical field

$$\psi(\mathbf{x},t) = \tilde{\psi}(\mathbf{x},t) \text{ on } \Gamma_p$$
$$D_i n_i = \tilde{Q}(\mathbf{x},t) \text{ on } \Gamma_q \tag{8}$$

where Γ_u, Γ_t, Γ_p, Γ_q are respectively parts of the global boundary Γ with prescribed displacements $\tilde{u}_i(\mathbf{x},t)$, tractions $\tilde{T}_i(\mathbf{x},t)$, electric potential $\tilde{\psi}(\mathbf{x},t)$ and surface density of electric induction field flux $\tilde{Q}(\mathbf{x},t)$ (normal component of electric displacements).

Constitutive equations (3) and (4) may be rewritten for transversally isotropic piezoelectric material that has hexagonal material symmetry and is poled in the x_3-direction as

$$\sigma_{11} = c_{11}\varepsilon_{11} + c_{12}\varepsilon_{22} + c_{13}\varepsilon_{33} - e_{31}E_3 \tag{9}$$

$$\sigma_{22} = c_{12}\varepsilon_{11} + c_{22}\varepsilon_{22} + c_{23}\varepsilon_{33} - e_{31}E_3 \tag{10}$$

$$\sigma_{33} = c_{13}\varepsilon_{11} + c_{23}\varepsilon_{22} + c_{33}\varepsilon_{33} - e_{33}E_3 \tag{11}$$

$$\sigma_{23} = c_{44}2\varepsilon_{23} - e_{15}E_2 \tag{12}$$

$$\sigma_{13} = c_{55}2\varepsilon_{13} - e_{15}E_1 \tag{13}$$

$$\sigma_{12} = c_{66}2\varepsilon_{12} \tag{14}$$

$$D_1 = e_{15}2\varepsilon_{13} + h_{11}E_1 \tag{15}$$

$$D_2 = e_{15}2\varepsilon_{23} + h_{22}E_2 \tag{16}$$

$$D_3 = e_{31}\varepsilon_{11} + e_{31}\varepsilon_{22} + e_{33}\varepsilon_{33} + h_{33}E_3 \tag{17}$$

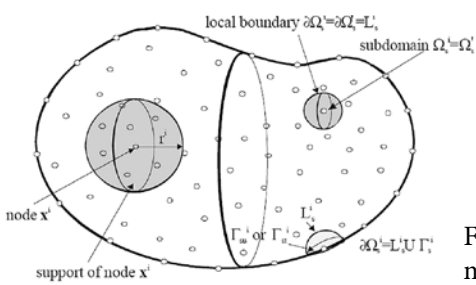

Figure 2. Local boundaries and subdomain for weak formulation and support domain for MLS approximation

Local weak forms of the governing equations (1, 2) used in the MLPG formulations are defined over local subdomains Ω_s as follows

$$\int_{\Omega_S} \sigma_{ij,j}(\mathbf{x},t)\, w_{ik}^{*}(\mathbf{x})\, d\Omega - \int_{\Omega_S} \rho \ddot{u}_i(\mathbf{x},t)\, w_{ik}^{*}(\mathbf{x})\, d\Omega = -\int_{\Omega_S} X_i(\mathbf{x},t)\, w_{ik}^{*}(\mathbf{x})\, d\Omega \tag{18}$$

$$\int_{\Omega_S} D_{j,j}(\mathbf{x},t)\, w^{*}(\mathbf{x})\, d\Omega + \int_{\Omega_S} R(\mathbf{x},t)\, w^{*}(\mathbf{x})\, d\Omega = 0 \tag{19}$$

where $\partial\Omega_s$ is the boundary of the local subdomain, which consists of five parts $\partial\Omega_s = L_s \cup \Gamma_{su} \cup \Gamma_{st} \cup \Gamma_{sp} \cup \Gamma_{sq}$ (see Fig. 2). L_s is the local boundary that is totally inside global domain, Γ_{st} is the part of the local boundary that coincides with the global traction boundary, i.e., $\Gamma_{st} = \partial\Omega_s \cap \Gamma_t$, and similarly Γ_{su} is the part of the local boundary that coincides with the global displacement boundary, i.e. $\Gamma_{su} = \partial\Omega_s \cap \Gamma_u$. Analogously $\Gamma_{sp} = \partial\Omega_s \cap \Gamma_p$ and $\Gamma_{sq} = \partial\Omega_s \cap \Gamma_q$.

Unit step functions $w_{ik}^{*}(\mathbf{x})$ and $w^{*}(\mathbf{x})$ are chosen as test functions in each subdomain and are defined as

$$w_{ik}^{*}(\mathbf{x}) = \begin{cases} \delta_{ik} \text{ at } \mathbf{x} \in (\Omega_s \cup \partial\Omega_s) \\ 0 \text{ at } \mathbf{x} \notin (\Omega_s \cup \partial\Omega_s) \end{cases}, \quad w^{*}(\mathbf{x}) = \begin{cases} 1 \text{ at } \mathbf{x} \in (\Omega_s \cup \partial\Omega_s) \\ 0 \text{ at } \mathbf{x} \notin (\Omega_s \cup \partial\Omega_s) \end{cases} \tag{20}$$

Applying the Gauss divergence theorem to eqs. (18, 19) and making use of eq. (20) one obtains the following local integral equations (LIEs)

$$\int_{\partial\Omega_S} \sigma_{ij}(\mathbf{x},t)\, n_j(\mathbf{x})\, d\Gamma - \int_{\Omega_S} \rho \ddot{u}_i(\mathbf{x},t)\, d\Omega = -\int_{\Omega_S} X_i(\mathbf{x},t)\, d\Omega \tag{21}$$

$$\int_{\partial\Omega_S} D_j(\mathbf{x},t)\, n_j(\mathbf{x})\, d\Gamma + \int_{\Omega_S} R(\mathbf{x},t)\, d\Omega = 0 \tag{22}$$

where $n_j(\mathbf{x})$ is the unit outward normal vector to the boundary $\partial\Omega_s$.

Eqs. (21, 22) may be rewritten for each component, assuming vanishing body forces $X_i(\mathbf{x}, t)$ and volume density of free electric charges $R(\mathbf{x}, t)$.

$$\int_{\partial\Omega_S} \left[\sigma_{11}(\mathbf{x},t) n_1(\mathbf{x}) + \sigma_{12}(\mathbf{x},t) n_2(\mathbf{x}) + \sigma_{13}(\mathbf{x},t) n_3(\mathbf{x})\right] d\Gamma - \int_{\Omega_S} \rho \ddot{u}_1(\mathbf{x},t)\, d\Omega = 0 \tag{23}$$

$$\int_{\partial\Omega_S} \left[\sigma_{12}(\mathbf{x},t) n_1(\mathbf{x}) + \sigma_{22}(\mathbf{x},t) n_2(\mathbf{x}) + \sigma_{23}(\mathbf{x},t) n_3(\mathbf{x})\right] d\Gamma - \int_{\Omega_S} \rho \ddot{u}_2(\mathbf{x},t)\, d\Omega = 0 \tag{24}$$

$$\int_{\partial\Omega_S} \left[\sigma_{13}(\mathbf{x},t) n_1(\mathbf{x}) + \sigma_{23}(\mathbf{x},t) n_2(\mathbf{x}) + \sigma_{33}(\mathbf{x},t) n_3(\mathbf{x})\right] d\Gamma - \int_{\Omega_S} \rho \ddot{u}_3(\mathbf{x},t)\, d\Omega = 0 \tag{25}$$

$$\int_{\partial\Omega_S} \left[D_1(\mathbf{x},t) n_1(\mathbf{x}) + D_2(\mathbf{x},t) n_2(\mathbf{x}) + D_3(\mathbf{x},t) n_3(\mathbf{x}) \right] d\Gamma = 0 \tag{26}$$

In general, a meshless method uses a local interpolation to represent the trial function with the values (or the fictitious values) of the unknown variable at some randomly located nodes. The moving least-squares (MLS) approximation (Lancaster and Salkauskas, 1981; Nayroles et al., 1992) used in our analysis may be considered as such scheme. According to the MLS method (Atluri, 2004), the approximation of displacements $u_j(\mathbf{x}, t)$ and electric potential $\psi(\mathbf{x}, t)$ by approximants $u_j^h(\mathbf{x},t)$, $\psi^h(\mathbf{x},t)$, is given by

$$u_j(\mathbf{x},t) \cong u_j^h(\mathbf{x},t) = \sum_{i=1}^{n} \phi^i(\mathbf{x}) \hat{u}_j^i(t) \tag{27}$$

$$\psi(\mathbf{x},t) \cong \psi^h(\mathbf{x},t) = \sum_{i=1}^{n} \phi^i(\mathbf{x}) \hat{\psi}^i(t) \tag{28}$$

where the nodal values $\hat{u}_j^i(t)$, $\hat{\psi}^i(t)$ are referred to as fictitious parameters for the displacements and electric potential, and $\phi^i(\mathbf{x})$ is called MLS shape function defined over n nodes located in a support domain Ω_x of the MLS approximation as shown in Figure 2.

The appropriate derivatives can be obtained with use of the shape function derivative as shown in (Atluri, 2004). Derivatives of displacements and electric potential are then given as

$$u_{j,k}^h(\mathbf{x},t) = \sum_{i=1}^{n} \phi_{,k}^i(\mathbf{x}) \hat{u}_j^i(t) \tag{29}$$

$$\psi_{,k}^h(\mathbf{x},t) = \sum_{i=1}^{n} \phi_{,k}^i(\mathbf{x}) \hat{\psi}^i(t) \tag{30}$$

Applying eqs. (27 – 30) for the spatial approximation of trial functions $u_j(\mathbf{x}, t)$, $\psi(\mathbf{x}, t)$ and their derivatives in constitutive relations (9 – 17) and their subsequent insertion into local integral equations (23 – 26) yields discretized local integral equations in the following form

$$\begin{aligned}
&\sum_{i=1}^{n} \hat{u}_1^i \left(\int_{\partial\Omega_S} \left[n_1 c_{11} \phi_{,1}^i(\mathbf{x}) + n_2 c_{66} \phi_{,2}^i(\mathbf{x}) + n_3 c_{55} \phi_{,3}^i(\mathbf{x}) \right] d\Gamma \right) - \sum_{i=1}^{n} \ddot{\hat{u}}_1^i \left(\int_{\Omega_S} \rho \phi^i(\mathbf{x}) d\Omega \right) + \\
&+ \sum_{i=1}^{n} \hat{u}_2^i \left(\int_{\partial\Omega_S} \left[n_1 c_{12} \phi_{,2}^i(\mathbf{x}) + n_2 c_{66} \phi_{,1}^i(\mathbf{x}) \right] d\Gamma \right) + \sum_{i=1}^{n} \hat{u}_3^i \left(\int_{\partial\Omega_S} \left[n_1 c_{13} \phi_{,3}^i(\mathbf{x}) + n_3 c_{55} \phi_{,1}^i(\mathbf{x}) \right] d\Gamma \right) + \\
&+ \sum_{i=1}^{n} \hat{\psi}^i \left(\int_{\partial\Omega_S} \left[n_1 e_{31} \phi_{,3}^i(\mathbf{x}) + n_3 e_{15} \phi_{,1}^i(\mathbf{x}) \right] d\Gamma \right) = 0
\end{aligned} \tag{31}$$

$$\sum_{i=1}^{n}\hat{u}_1^i\left(\int_{\partial\Omega_S}\left[n_1c_{66}\phi_{,2}^i(\mathbf{x})+n_2c_{12}\phi_{,1}^i(\mathbf{x})\right]d\Gamma\right)-\sum_{i=1}^{n}\hat{\ddot{u}}_2^i\left(\int_{\Omega_S}\rho\phi^i(\mathbf{x})d\Omega\right)+$$
$$+\sum_{i=1}^{n}\hat{u}_2^i\left(\int_{\partial\Omega_S}\left[n_1c_{66}\phi_{,1}^i(\mathbf{x})+n_2c_{22}\phi_{,2}^i(\mathbf{x})+n_3c_{44}\phi_{,3}^i(\mathbf{x})\right]d\Gamma\right)+$$
$$+\sum_{i=1}^{n}\hat{u}_3^i\left(\int_{\partial\Omega_S}\left[n_2c_{23}\phi_{,3}^i(\mathbf{x})+n_3c_{44}\phi_{,2}^i(\mathbf{x})\right]d\Gamma\right)+ \tag{32}$$
$$+\sum_{i=1}^{n}\hat{\psi}^i\left(\int_{\partial\Omega_S}\left[n_2e_{31}\phi_{,3}^i(\mathbf{x})+n_3e_{15}\phi_{,2}^i(\mathbf{x})\right]d\Gamma\right)=0$$

$$\sum_{i=1}^{n}\hat{u}_1^i\left(\int_{\partial\Omega_S}\left[n_1c_{55}\phi_{,3}^i(\mathbf{x})+n_3c_{13}\phi_{,1}^i(\mathbf{x})\right]d\Gamma\right)+\sum_{i=1}^{n}\hat{u}_2^i\left(\int_{\partial\Omega_S}\left[n_2c_{44}\phi_{,3}^i(\mathbf{x})+n_3c_{23}\phi_{,2}^i(\mathbf{x})\right]d\Gamma\right)+$$
$$+\sum_{i=1}^{n}\hat{u}_3^i\left(\int_{\partial\Omega_S}\left[n_1c_{55}\phi_{,1}^i(\mathbf{x})+n_2c_{44}\phi_{,2}^i(\mathbf{x})+n_3c_{33}\phi_{,3}^i(\mathbf{x})\right]d\Gamma\right)-\sum_{i=1}^{n}\hat{\ddot{u}}_3^i\left(\int_{\Omega_S}\rho\phi^i(\mathbf{x})d\Omega\right)+ \tag{33}$$
$$+\sum_{i=1}^{n}\hat{\psi}^i\left(\int_{\partial\Omega_S}\left[n_1e_{15}\phi_{,1}^i(\mathbf{x})+n_2e_{15}\phi_{,2}^i(\mathbf{x})+n_3e_{33}\phi_{,3}^i(\mathbf{x})\right]d\Gamma\right)=0$$

$$\sum_{i=1}^{n}\hat{u}_1^i\left(\int_{\partial\Omega_S}\left[n_1e_{15}\phi_{,3}^i(\mathbf{x})+n_3e_{31}\phi_{,1}^i(\mathbf{x})\right]d\Gamma\right)+\sum_{i=1}^{n}\hat{u}_2^i\left(\int_{\partial\Omega_S}\left[n_2e_{15}\phi_{,3}^i(\mathbf{x})+n_3e_{31}\phi_{,2}^i(\mathbf{x})\right]d\Gamma\right)+$$
$$+\sum_{i=1}^{n}\hat{u}_3^i\left(\int_{\partial\Omega_S}\left[n_1e_{15}\phi_{,1}^i(\mathbf{x})+n_2e_{15}\phi_{,2}^i(\mathbf{x})+n_3e_{33}\phi_{,3}^i(\mathbf{x})\right]d\Gamma\right)+ \tag{34}$$
$$+\sum_{i=1}^{n}\hat{\psi}^i\left(\int_{\partial\Omega_S}\left[n_1h_{11}\phi_{,1}^i(\mathbf{x})+n_2h_{22}\phi_{,2}^i(\mathbf{x})+n_3h_{33}\phi_{,3}^i(\mathbf{x})\right]d\Gamma\right)=0$$

Collecting the discretized local integral equations (31 – 34) together with the discretized boundary conditions gives a complete system of ordinary differential equations (ODEs) which can be rearranged such that all known quantities are on the r.h.s. Thus, in the matrix form the system becomes

$$\mathbf{M}\ddot{\mathbf{y}}+\mathbf{K}\mathbf{y}=\mathbf{f} \tag{35}$$

where the vector $\mathbf{y}$ is defined as $\mathbf{y}=\left\{\hat{u}_1^a(t),\hat{u}_2^a(t),\hat{u}_3^a(t),\hat{\psi}^a(t)\right\}^T$, $a = 1,\ldots N_t$. N_t is the total number of nodes. This system of ODEs can be solved by the Houbolt finite-difference scheme (Houbolt, 1950). In this method the "acceleration" term is defined as

$$\ddot{\mathbf{y}}_{t+\Delta t} = \frac{2\mathbf{y}_{t+\Delta t} - 5\mathbf{y}_t + 4\mathbf{y}_{t-\Delta t} - \mathbf{y}_{t-2\Delta t}}{\Delta t^2} \tag{36}$$

where Δt is the time step. Substituting eq. (36) into eq. (35) gives the system of algebraic equations for the unknowns $\mathbf{y}_{t+\Delta t}$

$$\left[\frac{2}{\Delta t^2}\mathbf{M} + \mathbf{K}\right]\mathbf{y}_{t+\Delta t} = \frac{1}{\Delta t^2}5\mathbf{M}\mathbf{y}_t + \mathbf{M}\frac{1}{\Delta t^2}\left\{-4\mathbf{y}_{t-\Delta t} + \mathbf{y}_{t-2\Delta t}\right\} + \mathbf{f} \tag{37}$$

The value of the time-step has to be appropriately selected with respect to material parameters (elastic wave velocities). Under quasi-electrostatic conditions the electric response is immediate as electric disturbances propagate with the speed of light.

3. Numerical examples

Numerical examples involving uniform and non-uniform compressive loads are used to test the proposed MLPG formulation. The results obtained are also compared to the FEM solution given by the ANSYS commercial finite element code. A cylindrical piezoelectric sensor with radius $r = 0.015$ m and thickness $h = 0.003$ m is considered. The bottom of the sensor is mechanically clamped with vanishing electric potential. The sensor is discretized with 1005 nodal points. Homogeneous and functionally graded material properties are considered. The material properties of PZT-4 piezoelectric ceramics given in Table 1 are assumed. A compressive load is applied from the top and the side is traction free.

Table 1. Mechanical and electrical properties of materials considered

Material property	value	material property	value
c_{11} [N m^{-2}]	13.9×10^{10}	e_{15} [C m^{-2}]	12.7
c_{12} [N m^{-2}]	7.78×10^{10}	e_{31} [C m^{-2}]	-5.2
c_{13} [N m^{-2}]	7.43×10^{10}	e_{33} [C m^{-2}]	15.1
c_{33} [N m^{-2}]	11.5×10^{10}	h_{11} [C(Vm)$^{-1}$]	6.46×10^{-9}
c_{44} [N m^{-2}]	2.56×10^{10}	h_{33} [C(Vm)$^{-1}$]	5.62×10^{-9}
r [kg m^{-3}]	7500		

In the first numerical example, a uniform static compressive load $\bar{T}_3\left(x_1, x_2, x_3 = h\right) = -1\times10^6 \left\lfloor \mathrm{N/m^2} \right\rfloor$ is assumed for the sensor with homogeneous material properties. Figure 3 shows the resulting vertical displacement and Figure 4 depicts the electric potential variation at the top of the sensor. Note that this response is axially symmetric with respect to the vertical x_3 – axis. The results are in excellent agreement with the FEM solution.

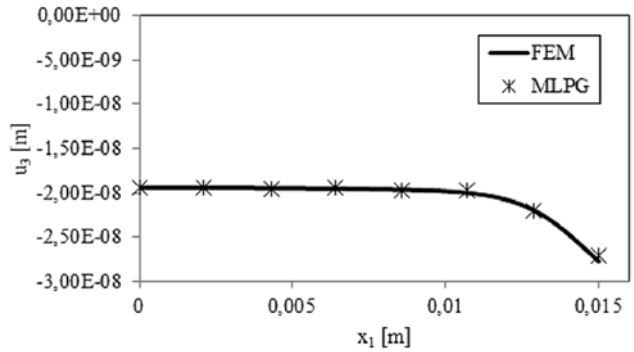

Figure 3. Variation of vertical displacement at the top of the sensor with x_1 – coordinate

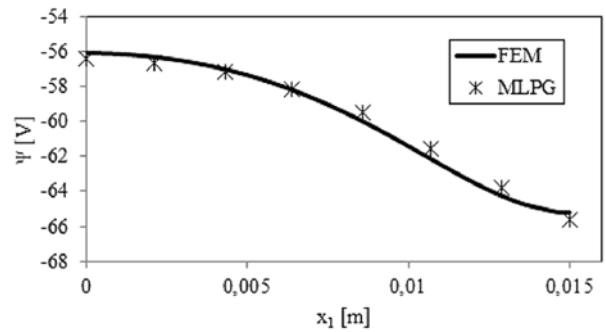

Figure 4. Variation of electric potential at the top of the sensor with x_1 – coordinate

A uniform compressive load with prescribed displacement field $\tilde{u}_3\left(x_1, x_2, x_3 = h\right) = -1\times10^{-8}\ \left[\mathrm{m}\right]$ is considered next. The response of the electric potential at the top of the sensor is shown in Figure 5. There is a significant difference in the shape of the response curves of electric potential when Figures 4 and 5 are compared.

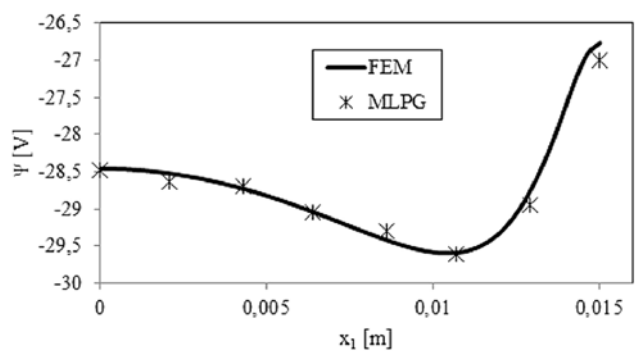

Figure 5. The electric potential response at the top of the sensor to prescribed uniform displacement load

The 3-D model of the piezoelectric sensor is suitable for the analysis of the prescribed non-uniform load usually found in practice. A vertical traction load varying linearly with the x_1 coordinate is applied in the next example as $\tilde{T}_3\left(x_1, x_2, x_3 = h\right) = -1e^6 - 5e^7 x_1 \left[\mathrm{N/m^2}\right]$. The non-uniform and non-symmetric load pattern produces a non-uniform response. Figure 6 shows the vertical displacement response to the compressive load, while Figure 7 shows the electric potential response.

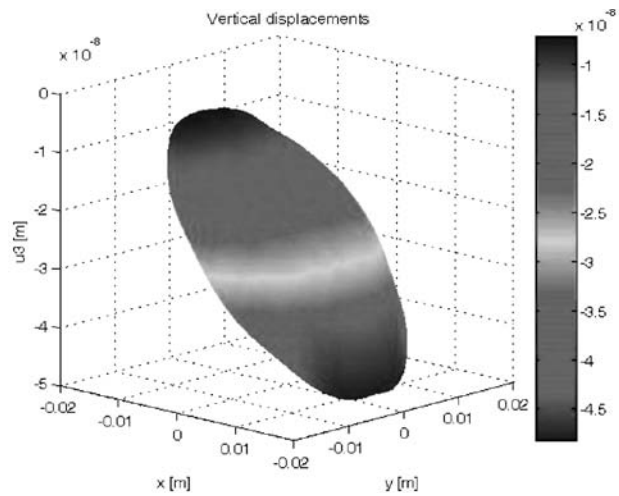

Figure 6. Vertical displacement at the top of the sensor under non-uniform load.

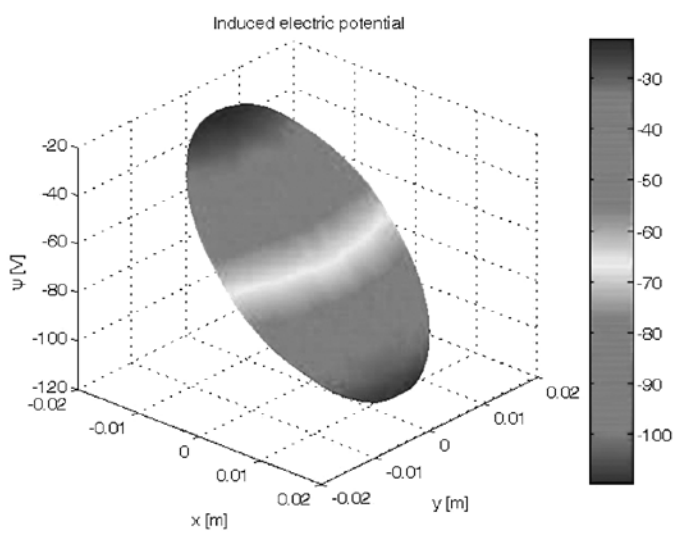

Figure 7. Induced electric potential at the top of the sensor under non-uniform load for homogeneous material properties

Functionally graded material properties are also considered for the analysis. The exponential gradation of elastic material constants is governed by

$$P(\mathbf{x}) = P_0\left(d - \exp(\gamma z)\right) \tag{38}$$

where the symbol P is commonly used for particular material coefficients and P_0 represents the material parameters on the upper surface of the FG layer. Gradation coefficient γ and constant d determine the shape of the exponential curve. Grading constants are chosen as $\gamma = -231.05$, $d = 1.5$, which represent the material properties at the bottom, reduced to half the value of the properties at the top of the sensor. Meanwhile, the piezoelectric properties are graded according to this formula

$$P(z) = P_0 \exp\left(\delta z / h\right) \tag{39}$$

where $\delta = 0.405$, which represents the 1.5-times increase in the value at the top relative to the bottom of the sensor. The resulting electric potential response at the top of the FGM sensor is shown in Figure 8. Higher electric potential values are induced than in the homogeneous case shown in Figure 7.

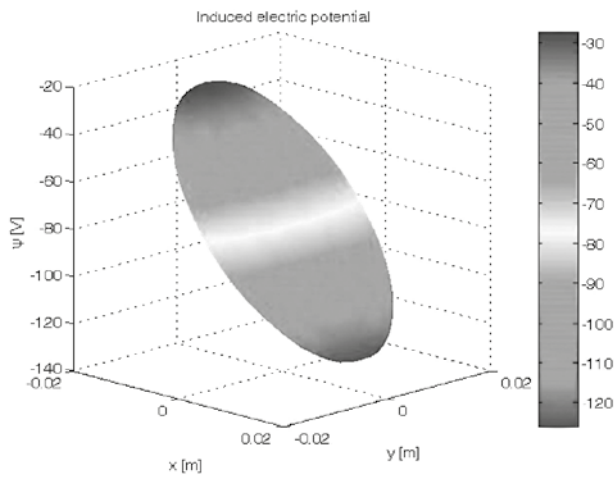

Figure 8. Induced electric potential at the top of the sensor under non-uniform load for FGM material properties

Finally, transient loading is assumed for the sensor with homogeneous material properties. A uniform transient compressive load with amplitude $\tilde{T}_3\left(x_1, x_2, x_3 = h, t\right) = -1\times10^6\ \left[\mathrm{N/m^2}\right]$ and Heaviside step time variation is considered. The Houbolt finite difference scheme is utilized. 100 time steps were applied for time interval 0 - 1.5×10^{-6} sec. The resulting vertical displacement at the center of the top is shown in Figure 9. The time variation of the induced electric potential is shown for the same point in Figure 10. Note that maximum peak values are approximately double the results for the static case shown in Figures 3 and 4. Since no damping is present, the solution will oscillate in the same fashion until infinity.

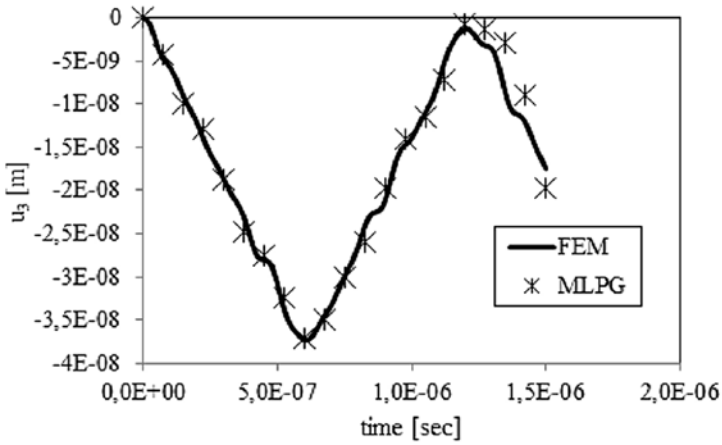

Figure 9. Time variation of vertical displacement at the center top of the piezoelectric sensor

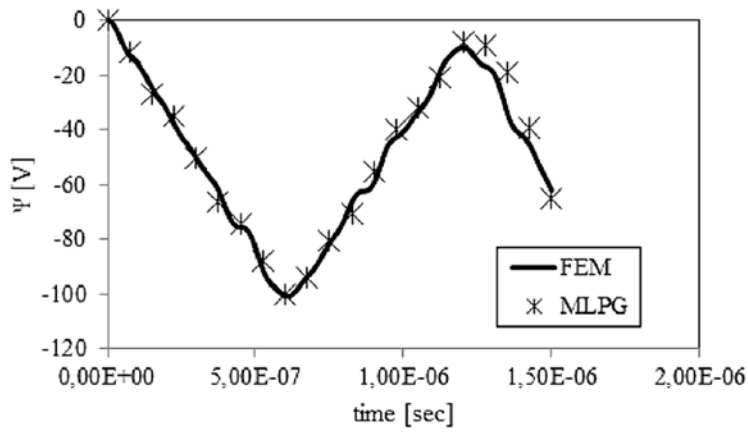

Figure 10. Time variation of electric potential at the center top of the piezoelectric sensor

4. Conclusions

A cylindrical piezoelectric sensor was analyzed by the MLPG method. Both static and transient dynamic loads were considered. Axisymmetric analysis is not applicable to non-uniform and non-symmetric loading and so a general 3-D analysis has to be performed. The cylindrical geometry of the sensor is discretized in terms of nodal points only. Each node is surrounded by a small spherical subdomain. A Heaviside unit step function was used as the test function in the derivation of local integral equations. The moving least-squares (MLS) scheme was adopted for the spatial approximations of the mechanical and electrical fields. Regarding the development of the MLPG formulation, the method presented is particularly promising for problems which cannot be solved by the conventional BEM, for example, when fundamental solutions are not available. However, in its current development, the proposed method requires more computational time since there are many more nodes involved and the shape functions in the MLS approximation are significantly more com-

plex than in the BEM or FEM using simple polynomials. Intensive research has been carried out to reduce the CPU time (Soares et al., 2012). Applications to similar problems for analysis of 3-D problems are expected in the future.

The present meshless formulation has a great potential for modeling continuously non-homogeneous materials, smart materials and other multi-field problems including piezothermoelasticity or magneto-electro-elasticity.

Acknowledgements

The authors gratefully acknowledge the support of the Slovak Science and Technology Assistance Agency registered under number APVV-0014-10.

REFERENCES

[1] Adachi, A., Kitamura, Y. and Iwatsubo, T. (2004), "Integrated design of piezoelectric damping system for flexible structure", Applied acoustics, 65, 293-310.

[2] Allik, H. and Hughes, T. J. R. (1970), "Finite element method for piezoelectric vibration", Int. J Numer. Methods Engng, 2, 151-157.

[3] Atluri, S. N. (2004), *The meshless method (MLPG)for domain & BIE discretizations*, Tech. Science Press, Forsyth, USA.

[4] Atluri, S. N. and Sladek, J. (Eds.) (2009), *Advances in the MLPG Meshless Methods*, Tech. Sci. Press, Duluth.

[5] Benjeddou, A. (2000), "Advances in piezoelectric finite element modeling of adaptive structural elements: a survey", Computers and Structures 76, 347-363.

[6] Ching H. K. and Batra R.C. (2001), "Determination of Crack Tip Fields in Linear Elastostatics by the Meshless Local Petrov-Galerkin (MLPG) Method", Computer Modeling in Engineering & Sciences, 2 (2), 273-289.

[7] Davi, G. and Milazzo, A. (2001), "Multidomain boundary integral formulation for piezoelectric materials fracture mechanics", Int. J. Solids Structures, 38, 2557-2574.

[8] Ding, H. and Liang, J. (1999), "The fundamental solutions for transversaly isotropic piezoelectricity and boundary element method", Computers & Structures 71, 447-455.

[9] Garcia-Sanchez, F., Rojas-Diaz, R., Saez, A. and Zhang, Ch. (2007), "Fracture of magneto-electroelastic composite materials using boundary element method (BEM)", Theoretical and Applied Fracture Mechanics 47, 192-204.

[10] Heyliger, P. (1997), "Exact solutions for simply supported laminated piezoelectric plates", J Appl Mech 64, 299-306.

[11] Houbolt, J. C. (1950), "A recurrence matrix solution for the dynamic response of elastic aircraft", Journal of Aeronautical Sciences 17, 371-376.

[12] Lancaster, P. and Salkauskas, T. (1981), "Surfaces generated by moving least square methods", Math. Comput. 37, 141-158.

[13] Lee, J. S. (1995), "Boundary element method for electroelastic interaction in piezoceramics", Engineering Analysis with Boundary Elements, 15, 321-328.

[14] Nayroles, B., Touzot, G. and Villon, P. (1992), "Generalizing the finite element method: diffuse approximation and diffuse elements", Comput. Mech., 10, 307-318.

[15] Nguyen, V. P., Rabczuk, T., Bordas, S. and Duflot, M. (2008), "Meshless methods: A review and computer implementation aspects", Mathematics and Computers in Simulation 79, 763-813.

[16] Pan, E. (1999), "A BEM analysis of fracture mechanics in 2D anisotropic piezoelectric solids", Engineering Analysis with Boundary Elements, 23, 67-76.
[17] Ray, M. C., Bhattacharya, R. and Samanta, B. (1998), "Exact solutions for dynamic analysis of composite plates with distributed piezoelectric layers", Computers and Structures 66, 737-743.
[18] Semedo Garção, J. E., Mota Soares, C. M., Mota Soares, C. A. and Reddy, J. N. (2004), "Analysis of laminated adaptive plate structures using layerwise finite element models", Computers and Structures 82, 1939-1959.
[19] Sladek, J., Sladek, V. and Mang, H. A. (2003), "Meshless LBIE formulations for simply supported and clamped plates under dynamic load", Computers and Structures, 81, 1643-1651.
[20] Sladek, J., Sladek, V. and Solek, P. (2009), "Elastic analysis in 3D anisotropic functionally graded solids by the MLPG", CMES: Computer Modeling in Engineering & Sciences, 43 (3), 223-251.
[21] Sladek, J., Sladek, V., Solek, P. and Saez, A. (2008), "Dynamic 3D axisymmetric problems in continuously non-homogeneous piezoelectric solids", International Journal of Solids and Structures 45, 4523-4542.
[22] Sladek, J., Sladek, V., Stanak, P. and Pan, E. (2010), "The MLPG for bending of electroelastic plates", CMES- Computer Modeling in Engineering & Sciences 64, 267-298.
[23] Sladek, J., Sladek, V., Stanak, P., Zhang, Ch. and Wunsche, M. (2013), "Analysis of the bending of circular piezoelectric plates with functionally graded material properties by a MLPG method", Engineering Structures, 47, 81-89.
[24] Soares, D. Jr., Sladek, V. and Sladek, J. (2012), "Modified meshless local Petrov-Galerkin formulations for elastodynamics", International Journal for Numerical Methods in Engineering, 90 (12), 1508-1528.
[25] Song, G., Sethi, V. and Li, H. N. (2006), "Vibration control of civil structures using piezoceramic smart materials: A review", Engineering Structures, 28, 1513-1524.
[26] Soric, J. and Jarak, T. (2010), "Mixed meshless formulation for analysis of shell-like structures", Comput. Methods Appl. Mech. Engrg., 199, 1153-1164.
[27] Stanak, P., Sladek, J., Sladek, V. and Krahulec S. (2011), "Composite circular plate analyzed as a 3-D axisymmetric piezoelectric solid", Building Research Journal 59, (3-4), 125-140.
[28] Tiersten, H. F. (1969), *Linear piezoelectric plate vibrations*, Plenum Press, New York.
[29] Vel, S. S. and Batra, R. C. (2000), "Three-dimensional analytical solution for hybrid multilayered piezoelectric plates", J Applied Mechanics, 67, 558-567.